

Progress in simulating turbulent electron thermal transport in NSTX

W. Guttenfelder¹, J.L. Peterson², J. Candy³, S.M. Kaye¹, Y. Ren¹, R.E. Bell¹, G.W. Hammett¹, B.P. LeBlanc¹, D.R. Mikkelsen¹, W.M. Nevins², H. Yuh⁴

¹ Princeton Plasma Physics Laboratory, Princeton NJ 08543

² Lawrence Livermore National Laboratory, Livermore, CA 94551

³ General Atomics, San Diego, CA 92186

⁴ Nova Photonics Inc., Princeton, NJ 08540

E-mail contact of main author: wgutten@pppl.gov

Abstract. Nonlinear simulations based on multiple NSTX discharge scenarios have progressed to help differentiate unique instability mechanisms and to validate with experimental turbulence and transport data. First nonlinear gyrokinetic simulations of microtearing (MT) turbulence in a high-beta NSTX H-mode discharge predict experimental levels of electron thermal transport that are dominated by magnetic flutter and increase with collisionality, roughly consistent with energy confinement times in dimensionless collisionality scaling experiments. Electron temperature gradient (ETG) simulations predict significant electron thermal transport in both low and high beta discharges when ion scales are suppressed by $E \times B$ shear. Although the predicted transport in H-modes is insensitive to variation in collisionality (inconsistent with confinement scaling), it is sensitive to variations in other parameters, particularly density gradient stabilization. In reverse shear (RS) L-mode discharges that exhibit electron internal transport barriers (e-ITBs), ETG transport has also been shown to be suppressed nonlinearly by strong negative magnetic shear, $s \ll 0$. In many high beta plasmas, TEM/KBM ballooning instabilities are found (simultaneous with MT) which scale like a trapped electron mode (TEM) except for the stiff beta dependence characteristic of kinetic ballooning modes (KBM). Nonlinear TEM/KBM simulations predict significant transport in all channels, with substantial contributions from compressional magnetic perturbations.

1. Introduction

While ion thermal transport is often neoclassical in spherical tokamaks (STs) such as National Spherical Torus Experiment (NSTX), electron thermal transport is always anomalous and can influence and limit the overall global energy confinement scaling [1,2]. To understand the cause of anomalous electron thermal transport due to microinstabilities driven by thermal plasma gradients (we do not address here the H-mode pedestal, or transport due to energetic particle instabilities such as GAEs [3]), nonlinear simulations are required to validate with experimental transport and turbulence measurements, to help distinguish unique instability mechanisms, and to improve predictive modeling capabilities.

STs can experimentally operate over a broad range of parameter space, spanning a significant range of beta, collisionality, toroidal flow/flow shear, and flux surface shaping. As a consequence, nonlinear simulations are challenging as it is unknown a priori what instability mechanisms are theoretically most important. To capture the correct qualitative physics it is crucial to account for many physical effects simultaneously, including: realistic equilibrium at low aspect ratio and high beta, fully electromagnetic (shear and compressional) perturbations, collisions, multiple kinetic species, and toroidal flow and flow shear.

Here we present recent progress in simulating microturbulence (using the Eulerian gyrokinetic code GYRO [4]) based on experimental NSTX discharges, with a focus predominantly on the observed anomalous electron thermal transport. The discharges include those from dedicated v_* confinement scaling studies [1,2,5], lithium deposition studies [6,7], and reverse magnetic shear (RS) discharges that exhibit strong electron internal transport barriers (e-ITBs) [8].

2. Linear survey

As an illustration of the range of experimental parameter space, Fig. 1 shows the values of electron beta (β_e) and collisionality (ν_{ei}) for a few NSTX NBI-heated H-mode discharges (at $r/a=0.6$) that are part of two separate v_* scaling experiments [1,5]. These scans operated at different line-averaged densities and neutral beam power, and therefore beta. The higher beta discharges are calculated to be unstable to the ion scale ($k_\theta \rho_s < 1$) microtearing mode (MTM), fundamentally an electromagnetic instability, with β_e above the linear threshold [9] (determined using linear calculations based on one high- v , high- β discharge). On the other hand, the low beta discharges are below the microtearing threshold, and instead the electron scale ($k_\theta \rho_s \gg 1$) ETG instability is predicted to be unstable [5]. To help differentiate instability mechanisms and to improve confidence in predictive modeling, nonlinear gyrokinetic simulations have been run to calculate the magnitude and scaling of the various instabilities.

3. Microtearing turbulence

First nonlinear gyrokinetic simulations of microtearing turbulence in NSTX have recently been reported (using deuterium only; ϕ , $A_{||}$; no flow/flow shear). These have been based on one of the high- v , high- β discharges in Fig. 1, which provides the somewhat idealized condition that MTM is the only unstable mode. As we will show later (Sec. 5), this is not always the case as other ion scale modes can often be present simultaneously further complicating the simulations.

Fig. 2 shows a snapshot of the resulting density ($\delta n/n_0$) and magnetic field (δB_r) fluctuations at a fixed toroidal angle in lab (R, Z) coordinates from a local simulation with a perpendicular domain $L_x \times L_y = 80 \times 100 \rho_s$, using $n_x/n_y = 540/16$ modes. (Other numerical resolutions are given in [10,11].) Narrow radial density perturbations are apparent on the outboard side, which correspond to the narrow resonant parallel current perturbations responsible for destabilizing the microtearing mode [11,12]. Resolving these perturbations requires narrow radial grid spacing ($\Delta x = 0.15 \rho_s$) that is capable of distinguishing the high order rational surfaces ($n_{\max} = 45$, $k_\theta \rho_{s, \max} = 0.945$) separated by $\Delta r_{\text{rat}, \min} = 1/n_{\max} q' = 1/k_{\theta, \max} S = 0.6 \rho_s$ ($S = r/q \cdot dq/dr = 1.75$).

While local peak density perturbations of $\delta n/n \sim 2\%$ occur around the entire poloidal circumference, the δB_r perturbations are strongly ballooning. The structure of δB_r is spatially broad on the outboard midplane with local instantaneous values as large as 30 Gauss

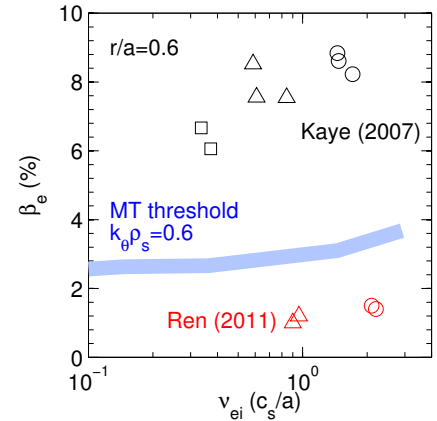


Fig. 1. Electron beta and collisionality (at $r/a=0.6$) for different NSTX shots (symbols), and calculated microtearing threshold using parameters from one discharge (line).

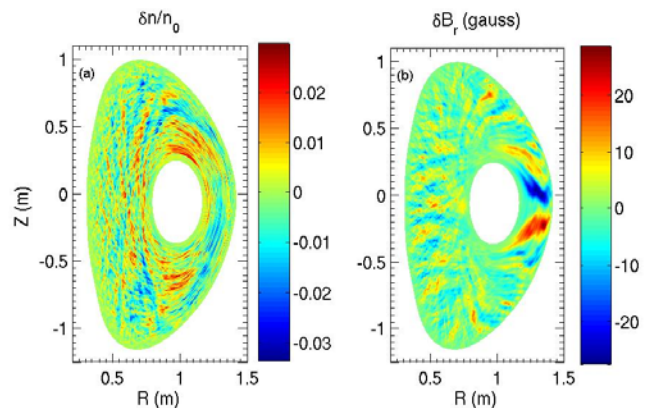


Fig. 2. (a) Normalized electron density and (b) δB_r (in Gauss) perturbations in a (R, Z) toroidal plane.

with local instantaneous values as large as 30 Gauss

($\sim 1\%$ of the vacuum field strength, $B_0=3.5\text{kG}$). Using both δn and δB_r from multiple time slices, calculations predict $1\text{-}2^\circ$ of instantaneous polarimetry phase shift ($\sim 0.3^\circ$ rms) dominated by δB_r , which may be measurable by a new polarimetry system [13] to be installed on NSTX-Upgrade.

The magnetic turbulence from the strong δB_r fluctuations leads to stochastic field line trajectories [11,14] and the corresponding magnetic flutter is responsible for almost all ($\sim 98\%$) of the electron thermal transport, $\chi_{e,\text{sim}} \approx 1.2 \rho_s c_s^2/a = 6 \text{ m}^2/\text{s}$, which is in the experimental range $\chi_{e,\text{exp}} = 5\text{-}8 \text{ m}^2/\text{s}$. Remarkably, the predicted transport increases with collisionality (Fig. 3, dots) with a scaling ($\chi_{e,\text{sim}} \sim v_e^{-1.1}$) that is roughly consistent with global energy confinement scaling in NSTX [1,2], $\Omega_i \tau_E \sim v_*^{-(0.8-0.95)}$, providing evidence for the importance of microtearing modes in determining confinement scaling in high-beta NSTX plasmas. When including experimental values of $E \times B$ shear ($\gamma_{E,\text{exp}} \approx 0.17 \text{ c}_s/a$, comparable to the maximum linear growth rate) the predicted transport is significantly reduced, complicating the above interpretation. Furthermore, MT transport is sensitive to variations in electron temperature gradient and beta, exhibiting thresholds in both parameters.

It was noted previously [11] that increasing both radial and binormal grid resolution may increase the transport quantitatively, possibly reconciling the apparent experimental discrepancy with finite $E \times B$ shear. However, such simulations require excessively large cpu time. Instead, more recently we have tested additional physical and numerical model assumptions based on the v_{ei} scaling, which are summarized in Fig. 3.

Linear studies based on these parameters find larger MT growth rates when including a second (carbon) impurity species (due to shielding of potential perturbations from the near-adiabatic ion response [9]). Consistent with linear analysis, nonlinear simulations including a carbon ion species show transport is reduced (Fig. 4) as carbon impurity is reduced ($n_c \rightarrow 0$, $Z_{\text{eff}} = 2.9 \rightarrow 1.0$), with the (early-time averaged) transport scaling similarly with collisionality (Fig. 3, diamonds). Later in time for the $n_c = 0$, $Z_{\text{eff}} = 1$ case the turbulence appears to transition from microtearing (with A_{\parallel} peaking at $k_{\theta} \rho_s \sim 0.3$) to instead a dominant electrostatic mode (with ϕ peaking at the lowest finite $k_{\theta} \rho_s = 0.1$). At these late times the ion thermal, particle and momentum fluxes are also increased due to potential perturbations. Simulations are ongoing to verify the robustness of this transition in turbulence regime to variations in numerical resolution.

Linear simulations also show that reducing the pressure gradient used in the equilibrium description [15] to match the thermal pressure (i.e. removing the fast ion contribution) increases width and maximum of the growth rate spectrum [9]. Consequently the resulting nonlinear transport (Fig.3, circle) is $>50\%$ larger than the base case.

The above simulations were run with fixed boundary conditions [4] to more conveniently include $E \times B$ shearing effects. The original scan (without $E \times B$ shear) was repeated using periodic boundary conditions (Fig. 3, squares), with transport that follows the same scaling

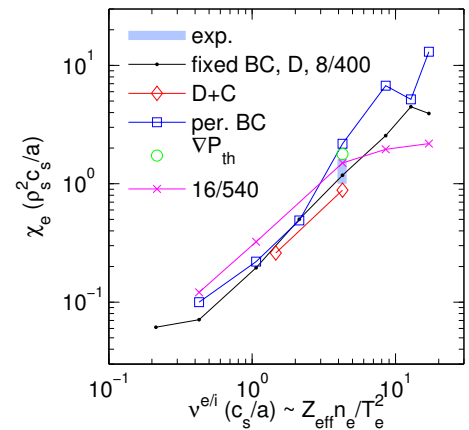


Fig. 3. Microtearing transport vs normalized electron-ion collision rate for different physical and numerical assumptions.

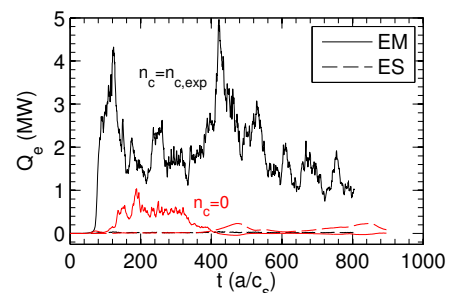


Fig. 4. MT transport from ϕ and A_{\parallel} for varying carbon concentration.

but at values 2-3 \times larger than that with fixed boundaries. We note that both fixed and periodic BC scans exhibit strongly bursting behavior at the highest collisionalities, likely due to the modest grid sizes ($L_x \times L_y = 80 \times 60$, $n_x/n_y = 400/8$). A limited set of higher resolution ($L_x \times L_y = 80 \times 100$, $n_x/n_y = 540/16$) simulations were also run (Fig. 3, \times), showing increase in transport for smaller collisionality, with a rollover at higher v_e^{*i} (and less bursty behavior) more consistent with the rollover in linear growth rates [9].

While the magnitude of transport around the experimental collisionality varies between $\chi_e = 0.9 - 2.2 \rho_s^2 c_s/a$, in all cases the general reduction of transport at reduced v_e^{*i} is robustly confirmed. Determining whether significant transport remains with experimental E \times B shear when using higher resolution, thermal pressure gradient, and periodic BCs (or wider perpendicular domain) awaits future simulations.

4. ETG turbulence

ETG is unstable in many NSTX discharges, often in locations where large E \times B shear is expected to suppress ion scale turbulence. We illustrate four cases below where ETG simulations have been run in an attempt to validate with experimental measurements.

The response of high- k turbulence to changes in local parameters has been studied using the coherent microwave scattering diagnostic [16]. In one set of experiments the local core density gradient was increased by about a factor of five as a consequence of a large ELM [17]. Both the measured high- k turbulence spectral power and local electron heat flux was reduced with the increasing density gradient. For the ‘‘pre-ELM’’ parameters, microtearing modes are stable and low- k ITG/TEM growth rates are comparable to or smaller than E \times B shearing rates. In this case,

local nonlinear ETG simulations (including D, C; ϕ , $A_{||}$, $B_{||}$; E \times B shear for low- k_0 cutoff and saturation [18]) predict transport approaching the experimental level ($Q_{e,exp} \sim 1.5 - 2.2$ MW) with $\sim 20\%$ increase in the experimental temperature gradient (Fig 5a). The fact that the ETG transport can be so large (\sim MW, $\chi_e \sim 20 \rho_e^2 v_{Te}/L_{Te}$) and stiff with

changes in a/L_{Te} confirms it can be important for some NSTX plasmas. Increasing the density gradient to ‘‘post-ELM’’ values dramatically reduces the transport (Fig. 5b, circles/squares), consistent with the experimental trend and expectations from linear stability [5,19]. However, the ETG transport predicted for the high density gradient case is considerably smaller than experiment. In this case, transport from trapped electron modes (TEM), driven by the increased density gradient, may provide a substantial contribution to the total transport.

The low beta experiments in Fig. 1 were carried out to vary electron collisionality (v_{e*}) by more than a factor of two with other normalized parameters kept relatively constant [5]. It is found that the measured high- k spectral power (in the region of $r/a = 0.55 - 0.7$) appears to increase with a reduction in collisionality, even though the normalized confinement time increases as $\Omega \tau^E \sim v_{e*}^{-0.8}$ (similar to high beta v_{e*} scans [2]). This anti-correlated dependence of the high- k turbulence with confinement is counterintuitive to expectations. Microtearing modes are predicted to be stable in these plasmas due to the lower values of beta, and local

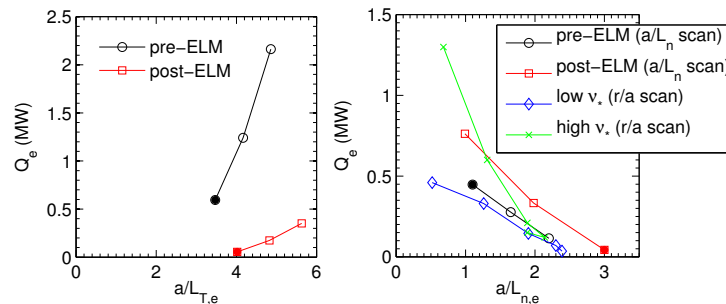


Fig. 5. (a) ETG heat flux vs. a/L_{Te} for pre-ELM (low a/L_{ne}) and post-ELM (high a/L_{ne}). (b) ETG heat flux vs. a/L_{ne} for pre/post-ELM, also for low/high- v_{*} shots (from r/a scan). Solid symbols represent experimental gradients.

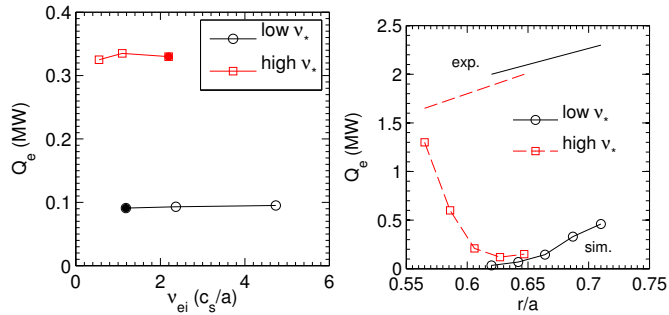


Fig. 6. For low and high v_* discharges: (a) ETG heat flux vs. normalized collision rate. (b) ETG heat flux vs. r/a .

that the accumulation of small differences in local parameters may lead to the overall change in confinement. Additional simulations at multiple locations that span the high- k measurement region ($r/a=0.56-0.71$, Fig. 6b) show the predicted transport changes substantially, and around $r/a \sim 0.55$ in the high v_* shot approaches the experimental values. While a number of parameters vary over this region (such as q and s , which are known to affect ETG transport through both linear [19] and nonlinear [20] scalings), the transport variation appears to be most strongly correlated with density gradient. This dependence (from the r/a scan) is shown in Fig. 5b (diamonds, \times 's) to behave very similarly to the density scaling from the pre/post-ELM discharge.

While the high beta discharges in Sec. 3 were unstable only to microtearing, ETG can play an important role in other high beta H-modes. Low- k_θ and high- k_θ growth rates calculated for five similar ‘‘pre-Lithium’’ discharges (129016-129020) that are part of the Li deposition studies [6,7] show that while microtearing modes are robustly unstable at low- $k_\theta \rho_s$ ($\gamma_{lin,MT} \sim 0.15-0.3 c_s/a$), they should be suppressed nonlinearly by the large local $E \times B$ shearing

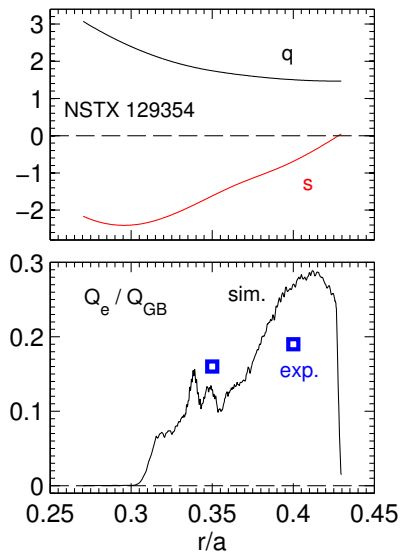


Fig. 8. (a) Safety factor (q) and magnetic shear (s) profiles for e-ITB discharge. (b) Nonlocal ETG electron heat flux.

$E \times B$ shearing rates are typically comparable to or larger than ITG/TEM growth rates [5]. Fig. 6a shows that the simulated local ETG transport ($Q_{e,sim} \sim 0.1-0.3$ MW) is much smaller than experimental transport ($Q_{e,exp} \sim 2$ MW), and is independent to variations in electron collisionality (expected from linear stability [5]), inconsistent with the global confinement scaling. We speculate

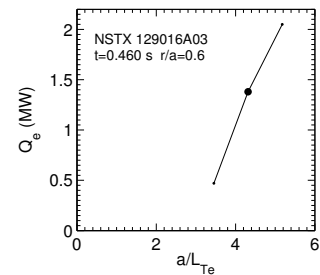


Fig. 7. ETG heat flux vs. temperature gradient.

rates ($\gamma_E \sim 0.76-0.91 c_s/a$). Nonlinear ETG simulations based on one of these discharges predicts significant transport ($Q_{e,sim} \sim 1.5$ MW compared to $Q_{e,exp} \sim 2$ MW), that is stiff with temperature gradient (Fig. 7), illustrating ETG can also play an important role in higher beta discharges.

Electron internal transport barriers (e-ITBs) have previously been reported to occur with strong negative magnetic shear ($s < -0.5$) in NSTX [8]. For a large collection of discharges, both the large local electron temperature gradients (much larger than the linear ETG threshold) and the small measured turbulence intensity from ‘‘high- k ’’ scattering are strongly correlated with the largest magnitudes of negative magnetic shear. Non-local GYRO simulations have verified that the ETG turbulence and transport is suppressed with strong negative magnetic shear in the region of the e-ITB, as shown in Fig. 8 [21]. In the outer regions of the e-ITB ($r/a > 0.3$) the predicted ETG flux reaches experimental levels but turbulence cannot propagate inward past the

barrier ($r/a \approx 0.3$).

Additional local simulations ($r/a=0.3$) at varying magnetic shear verify that this suppression can occur predominantly from a nonlinear stabilizing effect that occurs in the absence of strong $E \times B$ shear, confirming that negative magnetic shear alone is sufficient for ETG suppression. This nonlinear effect is very strong, with the threshold for significant transport ($R/L_{Te,NL} \sim 12-18$) approaching three times the linear critical gradient ($R/L_{Te,lin} \sim 4-6$) for values of s between $-0.2 \rightarrow -2.4$. This nonlinear upshift is significantly larger than the $\sim 30\%$ ‘‘Dimits’’ shift observed in some ITG simulations at conventional magnetic shear [22].

5. TEM/KBM turbulence

The analyses presented so far have focused on scenarios where it’s reasonable to consider transport mechanisms individually. Unfortunately, this is often not the case, particularly in high beta NSTX discharges in the region of $r/a=0.6-0.8$. To illustrate this, Fig 9a shows the linear growth rate spectra for a lithiated discharge (129041, [6,7]) at $r/a=0.7$, where a ballooning mode dominates the linear spectra with growth rates larger than the $E \times B$ shearing rate peaking around $k_{\theta} \rho_s \sim 0.35$, while a weaker microtearing mode spans a broader range peaking around $k_{\theta} \rho_s \sim 0.6$. (ETG is stable in this case.) Overlapping unstable spectra like these have been found in numerous NSTX linear stability simulations. Subsidiary scans (Fig. 9b) using the GYRO eigenvalue solver [15] show the ballooning mode exhibits many characteristics of a trapped electron mode (TEM) [23]: driven unstable by electron density and temperature gradients (a/L_n , a/L_{Te}), weakly dependent on ion temperature gradient (a/L_{Ti}), and strongly stabilized by increasing collisionality (ν_{ei}). The scaling with collisionality is opposite to that from microtearing, making it difficult to reconcile with the observed confinement scaling by considering variations in only one parameter.

Unlike a traditional electrostatic TEM instability, this mode is extremely sensitive to β_e with the appearance of an effective threshold ($\beta_{e,crit} \sim 0.8\%$) similar to that expected for a KBM instability [24]. The fact that the scaling of the growth rates are unified by the MHD alpha parameter (Fig. 9c), $\alpha_{MHD} = -q^2 R \nabla \beta$ [where $\beta = \Sigma (n_s T_s) \cdot 2\mu_0 / B_{unit}^2$], highlights the KBM nature of the instability. In addition, if compressional magnetic perturbations ($B_{||}$) are neglected (Fig. 9a, dashed line) the ballooning mode is stabilized. Given these characteristics we refer to this mode as a hybrid (or compressional) TEM/KBM. A similar collapse of γ vs. α_{MHD} at different radii has been observed in this and other discharges, illustrating the microinstabilities in NSTX can take on a KBM nature in the core confining region. Similar TEM/KBM behavior has also been predicted in GS2

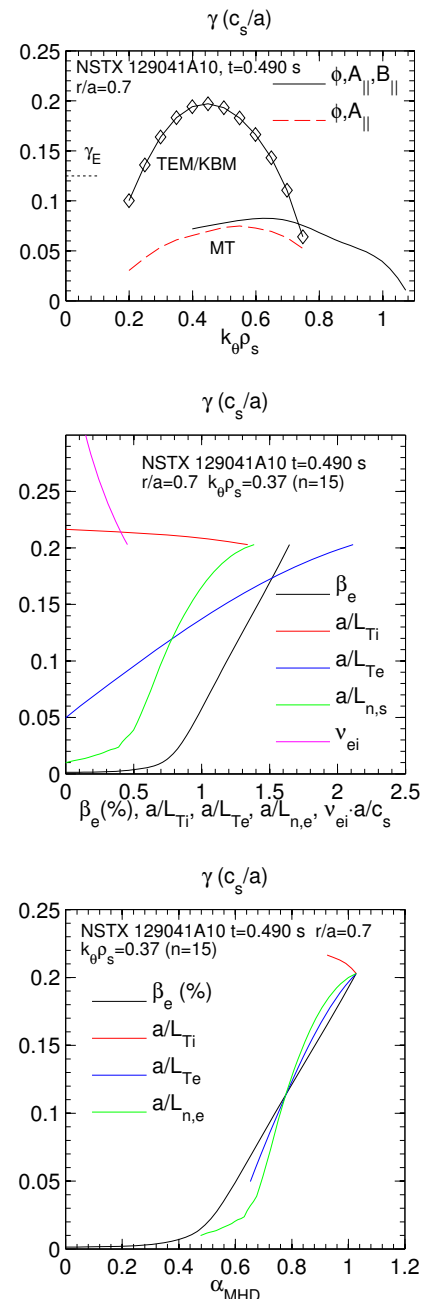


Fig. 9. (a) Linear spectra of overlapping MT and TEM/KBM. (b) Scaling of TEM/KBM growth rate vs. β_e , a/L_{Ti} , a/L_{Te} , a/L_n , ν_{ei} and (c) vs. α_{mhd} .

simulations further out in radius near the top, and inside of, the pedestal region of similar NSTX discharges [25].

Initial local nonlinear simulations based on this case ($L_x \times L_y = 69 \times 63 \rho_s$, $n_x = 140$, $n_y = 12$, $n_E = 8$, $n_\lambda = 12$, $n_\theta = 14 \times 2$, $dt = 0.001 a/c_s$; D,C; ϕ , A_{\parallel} , B_{\parallel} ; not including flow shear) show a number of interesting features (Fig. 10a). First, the predicted heat fluxes ($\sim 2-4$ MW) are experimentally significant ($P_{\text{NBI}} \sim 3$ MW) although the transport is very bursty (likely a consequence of the relatively small perpendicular domain). Second, there is a significant contribution to heat (and particle) fluxes from the B_{\parallel} perturbations (rms $\delta B_{\parallel}/B \sim 0.08\%$ for finite k_θ modes), consistent with the compressional nature of the linear instability. The time-averaged transport is reduced by half when scaling $\beta_e \times 0.5$ and is effectively eliminated for $\beta_e = 0$ (not shown), qualitatively following the linear stability scaling and confirming the importance of including finite beta in the simulations. The time-averaged transport fluxes peak around $k_\theta \rho_s \sim 0.3-0.4$ (Fig. 10b, solid lines) and decay at higher wavenumbers, although the finite residual values suggest higher binormal resolution is required for quantitative accuracy. One can also see around $t = 100-150 a/c_s$ there is a burst in electron thermal transport from the shear magnetic perturbations (A_{\parallel}) which eventually subsides. This is a consequence of the subdominant microtearing instability initially growing at higher $k_\theta \rho_s$, which is apparent from the early time contribution to the A_{\parallel} transport spectra in Fig. 10b (the contributions from ϕ and B_{\parallel} are similar to their late time values). Apparently in this case the microtearing turbulence is ultimately unable to compete with the stronger TEM/KBM turbulence, although convergence tests in radial resolution are required to verify the microtearing physics is sufficiently represented, as well as additional parameter scans to determine the regime of non-linear dominance and whether distinct modes can co-exist.

It is also interesting to note that when restarting the simulation using the local experimental values of toroidal flow and parallel flow shear ($Ma = 0.23$, $\gamma_p = 0.75 c_s/a$), the TEM/KBM turbulence predicts finite momentum transport, although in this particular case the turbulence is strongly reduced if the $E \times B$ shear is also included. Nevertheless, TEM/KBM, or overlapping TEM/KBM+MTM turbulence, provides one possible mechanism that could account for both anomalous electron and momentum transport in NSTX [26]. Additional simulations are underway to test the sensitivity of these predictions, and at other locations where $E \times B$ shear suppression is not as strong.

6. Summary and discussion

Nonlinear gyrokinetic simulations have been run for many NSTX discharges in order to validate with experimental measurements. The breadth of possible turbulence mechanisms highlights the importance of including all electromagnetic (shear and compressional) and collisional effects to capture the correct qualitative behavior. In high beta H-mode plasmas microtearing simulations predict experimental levels of electron thermal transport and scaling with collisionality consistent with energy confinement scaling, regardless of numerical and physical model. In some low and high beta H-modes (in regions of strong $E \times B$ shear) ETG

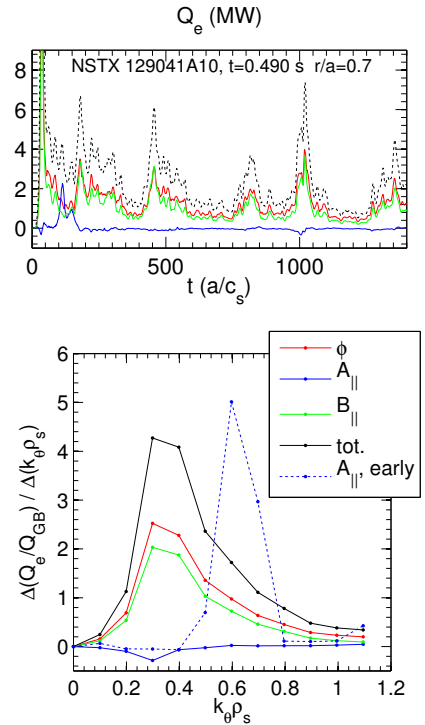


Fig. 10. (a) Time traces and (b) transport spectra for electron heat flux from TEM/KBM, separated into contributions from each field.

simulations can also predict significant electron thermal transport. Although ETG transport is independent of collisionality (inconsistent with confinement scaling) it is particularly sensitive to variations in the local density gradient (as well as variations in Z_{eff} , s , q). We speculate that the accumulation of small differences in these parameters influence the overall change in confinement. In reverse shear L-modes, ETG transport is suppressed (nonlinearly, in the absence of $E \times B$ shear) by strong negative magnetic shear in the region of the observed e-ITBs. In many high- β plasmas with sufficiently large α_{mhd} , compressional TEM/KBM instabilities are unstable, simultaneous with microtearing modes. These modes scale like TEM except for the strong β_e dependence. Nonlinear simulations predict significant transport in all channels (with nearly equal flux contributions from φ and B_{\parallel}), providing a mechanism to account for the anomalous momentum transport observed in NSTX. Future simulations will attempt to address how the overlapping of fundamentally different turbulence mechanisms influences the scaling of all transport channels.

This research used resources of the National Energy Research Scientific Computing Center, supported by U.S. DOE Contract DE-AC02-05CH11231, and the Oak Ridge Leadership Computing Facility, supported by DOE contract DE-AC05-00OR22725. This work was also supported by DOE contracts DE-AC02-09CH11466, DE-FG03-95ER54309, DE-AC52-07NA27344, and DE-FG02-99ER54527.

References

- [1] S.M. Kaye et al., Nucl. Fusion **47**, 499 (2007); Phys. Rev. Lett **98**, 175002 (2007).
- [2] S.M. Kaye et al., IAEA FEC EX-C/7-1(2012).
- [3] D. Stutman et al., Phys. Rev. Lett. **102**, 115002 (2009).
- [4] J. Candy and E. Belli, General Atomics Technical Report No. GA-A26818 (2010).
- [5] Y. Ren et al., Phys. Plasmas **19**, 056125 (2012).
- [6] R. Maingi et al., Phys. Rev. Lett. **107**, 145004 (2011).
- [7] R. Maingi et al., IAEA FEC EX/11-2 (2012).
- [8] H. Yuh et al., Phys. Rev. Lett. **106**, 055003 (2011).
- [9] W. Guttenfelder et al., Phys. Plasmas **19**, 022506 (2012).
- [10] W. Guttenfelder et al., Phys. Rev. Lett. **106**, 155004 (2011).
- [11] W. Guttenfelder, et al., Phys. Plasmas **19**, 056119 (2012).
- [12] R.D. Hazeltine, D. Dobrott, T.S. Wang, Phys. Fluids **18**, 1778 (1975).
- [13] J. Zhang et al., Rev. Sci. Instrum. **81**, 10D519 (2010).
- [14] E. Wang et al., Phys. Plasmas **18**, 056111 (2011).
- [15] E. Belli and J. Candy, Phys. Plasmas **17**, 112314 (2010); J. Candy, Plasma Phys. Control. Fusion **51**, 105009 (2009).
- [16] D.R. Smith et al., Rev. Sci. Instrum. **79**, 123501 (2008).
- [17] Y. Ren et al., Phys. Rev. Lett. **106**, 165005 (2011).
- [18] W. Guttenfelder and J. Candy, Phys. Plasmas **18**, 022506 (2011).
- [19] F. Jenko et al., Phys. Plasmas **9**, 4096 (2001).
- [20] F. Jenko, W. Dorland, Phys. Rev. Lett. **85**, 5579 (2000).
- [21] J.L. Peterson et al., Phys. Plasmas **19**, 056120 (2012).
- [22] A. Dimits et al., Phys. Plasmas **7**, 969 (2000).
- [23] A.G. Peeters et al., Phys. Plasmas **12**, 022505 (2005).
- [24] W.M. Tang et al., Nucl. Fusion **20**, 1439 (1980).
- [25] J.M. Canik et al., IAEA FEC EX/P7-16 (2012).
- [26] S.M. Kaye et al., Nucl. Fusion **49**, 045010 (2009).